JOURNAL OF COMPUTATIONAL PHYSICS 116, 300–313 (1994)

A Two-Dimensional Finite Element Model of the Edge Plasma

ROGER A. VESEY AND DON STEINER

Department of Nuclear Engineering and Engineering Physics, Rensselaer Polytechnic Institute, Troy, New York 12180

Received November 19, 1992; revised April 18, 1994

A new computational model of the edge plasma in axisymmetric magnetic fusion devices has been developed based on finite element methods. Braginskii-type plasma fluid equations and a one-energy-group neutral particle diffusion equation are spatially discretized on a two-dimensional domain using Galerkin, modified artificial diffusion, and anisotropic streamline-upwind/Petrov–Galerkin finite element methods. A damped modified Newton method is employed to solve the nonlinear system of discretized equations. Results from assembled plasma/neutral systems in rectangular geometry agree quantitatively with the results from the B2 and NEWEDGE finite-difference edge models and highlight the importance of boundary conditions. Finite element analysis of angled divertor plates illustrated the sensitivity of divertor plasma parameters and the divertor plate heat flux profile to the details of nonorthogonal boundary geometry, due to the neutral particle behavior and its subsequent effect on all of the plasma quantities. © 1995 Academic Press, Inc.

1. INTRODUCTION

The edge plasma in a magnetic fusion device (also referred to as the boundary plasma or scrape-off layer) is a region of transition between the high-temperature, dense core plasma and the physical walls of the vacuum vessel enclosing the plasma. A number of interrelated phenomena typically occur in the edge region of plasma devices. The energetic particle efflux and conductive energy flow from the core plasma provides the sources of particles and energy to the edge region. Particles are eventually removed by the active pumping of neutrals out of the vacuum vessel, while the plasma heat flux is removed by cooling the plasma-facing components. In general, a thorough understanding of edge plasma physics is necessary from both engineering and physics standpoints. Control of the particle and energy fluxes in the edge plasma is a critical design issue for high-power fusion devices such as the International Thermonuclear Experimental Reactor (ITER) [1].

Modeling of the edge plasma is therefore a critical and complex issue for near-term magnetic fusion devices. At this point, there is no comprehensive model incorporating all of the relevant physical processes. However, models of the edge plasma have evolved from analytical descriptions to one-dimensional single species models to two-dimensional multi-fluid models with realistic geometry. The primary two-dimensional edge plasma model in use today is B2, developed by Braams [2]. Features of the B2 code (in its most widely distributed form) include orthogonal curvilinear meshes, multiple ion species capability, analytic neutrals treatment, and diffusive cross-field transport. Vold [3] has presented results from his EPIC code which features orthogonal meshes generated from plasma equilibria, time-dependence, a relaxation technique similar to that used by Braams, and a one-group neutral particle diffusion model. The NEWEDGE code by Knoll [4], like the Braams model, uses finite volume discretization on an orthogonal mesh, but Newton's method is used to iteratively solve the system of nonlinear algebraic equations.

For finite difference techniques, at least a 9-point stencil is required to accurately include nonorthogonal geometry in two dimensions. To allow the use of more convenient 5-point finite difference stencils, the typically irregular geometry inherent to the edge region is often modeled as if the boundaries were parallel or perpendicular to the magnetic field, leading either to gross inaccuracies in the model boundary or to the use of stair-step boundaries. In either case, geometric inaccuracy is introduced in the region of greatest plasma/neutral activity. Also, the plasma-facing surface boundary conditions are the most complex, incorporating sheath physics and the treatment of neutral recycling processes. The primary motivation for considering finite element methods which (a) very naturally admit flexible geometry and (b) directly incorporate derivative-type boundary conditions, is therefore a desire to more accurately represent the recycling region boundary for limiter or divertor configurations.

Having introduced the essence of the edge modeling problem and the expected advantage of applying the finite element method, the remainder of the article is devoted to the development of a finite element plasma edge code. A summary of the preliminary assumptions and differential equations defining the edge physics model is given in Section II. Discussions of the relevant finite element methods, the resulting forms of the plasma edge equations, and the techniques used to solve the nonlinear discretized equations are presented in Section III. Extensive testing of the finite element code and an application to angled divertor plates are described in Section IV. Section V summarizes the capabilities of the present model as well as the areas for future improvement.

0021-9991/94 $6.00
Copyright © 1994 by Academic Press, Inc.
All rights of reproduction in any form reserved.

II. PHYSICS MODEL

Although a global model incorporating all relevant edge processes would be ideal, a tractable problem must limit its scope to a subset of the important phenomena. A number of basic assumptions have been made regarding the physics of the tokamak plasma edge for the purpose of developing the present model. These include:

(a) steady-state conditions apply,

(b) axisymmetry applies,

(c) the plasma is composed of a single hydrogenic ion species and electrons,

(d) the plasma is quasineutral (i.e., $n_e = n_i$),

(e) the plasma is current-free (i.e., $\mathbf{V}_e = \mathbf{V}_i$),

(f) plasma flow along magnetic field lines may be described by classical collisional theory,

(g) plasma flow transverse to magnetic field lines is diffusive and often anomalous in nature, and

(h) neutral particles are described by one-energy-group diffusion theory.

The five basic plasma variables considered by the current model are:

(a) n = ion density (m^{-3}),

(b) $u_\parallel$ = parallel ion fluid velocity (m s^{-1}),

(c) T_i = ion temperature (Joules),

(d) T_e = electron temperature (Joules), and

(e) n_o = neutral particle density (m^{-3}).

The equations presented below for the plasma fluid conservation relations are thus a simplification of the equations solved by Braams, which followed the treatment of Braginskii [5], allowing for particle sources. The rectangular coordinate system in which the equations are presented is oriented such that the x-axis is everywhere parallel to the poloidal magnetic field lines, while the y-axis is everywhere orthogonal to x (pointing in an outward approximately radial direction).

Particle balance.

$$\frac{\partial}{\partial x}(nu) + \frac{\partial}{\partial y}(nv) = S_n, \tag{1}$$

where

u = poloidal ion fluid velocity (x-velocity) (m s^{-1}),
v = transverse ion fluid velocity (y-velocity) (m s^{-1}),
S_n = ion source ($m^{-3}s^{-1}$).

The transverse ion flux, nv, is assumed to be diffusive in nature, given by the relation [2]

$$nv = -D_n \frac{\partial n}{\partial y} - \frac{D_p}{T_i}\frac{\partial}{\partial y}(nT_i) + nv_{\text{conv}}, \tag{2}$$

where

D_n = density gradient diffusion coefficient (m^2s^{-1}),
D_p = pressure gradient diffusion coefficient (m^2s^{-1}), and
v_{conv}= diffusion velocity due to other sources (ms^{-1}).

Parallel momentum balance.

$$m_i \nabla \cdot (nu_\parallel \mathbf{V}) - \nabla \cdot \eta \nabla u_\parallel = -\frac{B_\theta}{B}\frac{\partial}{\partial x}[n(T_i + T_e)], \tag{3}$$

where

m_i = ion mass (kg),
η = ion viscosity tensor (kg $m^{-2}s^{-1}$),
$\mathbf{V} = u\mathbf{e}_x + v\mathbf{e}_y$(m s^{-1}), and
B_θ/B = ratio of poloidal-to-total magnetic field.

Electron energy balance.

$$\nabla \cdot (\tfrac{5}{2}n\mathbf{V}T_e - \kappa_e \nabla T_e) = \mathbf{V} \cdot \nabla(nT_e) - k_{eq}(T_e - T_i) + S_E^e, \tag{4}$$

where

κ_e = electron thermal conductance tensor ($m^{-1}s^{-1}$),
k_{eq} = ion-electron temperature equilibration coefficient ($m^{-3}s^{-1}$), and
$S_E^e = \varepsilon_e S_n$ = electron energy source (J $m^{-3}S^{-1}$), and ε_e is the energy loss per ionization event.

Ion energy balance.

$$\begin{aligned}\nabla \cdot (\tfrac{5}{2}n\mathbf{V}T_i - \kappa_i \nabla T_i + \tfrac{1}{2}m_i n u_\parallel^2 \mathbf{V} - \tfrac{1}{2}\eta \nabla u_\parallel^2) \\ + \mathbf{V} \cdot \nabla(nT_e) - k_{eq}(T_e - T_i) = S_E^i,\end{aligned} \tag{5}$$

where

κ_i = ion thermal conductance tensor ($m^{-1}s^{-1}$), and
$S_E^i = \varepsilon_i S_n$ = ion energy source (J $m^{-3}S^{-1}$), and ε_i is the energy gain per ionization event.

Neutral particle diffusion. Vold [3] gives a complete derivation of the one-group neutral particle diffusion equation and the computational results which justify its use. The simple equation governing the neutral density, n_o, is

$$-\nabla \cdot D_{no} \nabla n_o = -S_n, \tag{6}$$

where

$D_{no} = 8T_i/3\pi n m_i(\langle\sigma v\rangle_{ie} + \langle\sigma v\rangle_{cx})$ = one-group neutral particle diffusion coefficient ($m^2 s^{-1}$)
$S_n = n n_o \langle\sigma v\rangle_{ie}$ = ionization sink for neutrals,
$\langle\sigma v\rangle_{ie}$ = the electron-impact ionization rate,
$\langle\sigma v\rangle_{cx}$ = the charge-exchange reaction rate.

It is the approximate solution of this system of highly nonlinear particle differential equations via the finite element method that is the subject of Section III.

III. NUMERICAL METHODS

A number of numerical techniques must be brought to bear upon the system of nonlinear differential equations defined in Section II to yield an approximate solution. This section will describe in some detail each of the various methods used. First, the finite element spatial discretization of a generic advection-diffusion equation is presented, including the standard Galerkin weak form, as well as upwind finite element methods. Next, the weak forms of the governing equations are described. Finally, the Newton iteration method is presented as a means to self-consistently solve the nonlinear discretized system of equations.

III.A. Finite Element Form of a Convection-Diffusion Equation

The first step in the solution of the given system of nonlinear partial differential equations via the finite element method is the derivation of weak forms of the equations. As an example, consider a general convection-diffusion problem, the strong form of which is stated as

Given $f(\mathbf{x})$, $\sigma(\mathbf{x})$, $\mathbf{a}(\mathbf{x})$, $\mathbf{K}(\mathbf{x})$, $\phi_g(\mathbf{x})$, and $\mathbf{q}(\mathbf{x})$, find ϕ:

$$\mathbf{a}\cdot\nabla\phi - \nabla\cdot\mathbf{K}\nabla\phi + \sigma\phi = f \quad \text{on } \Omega \tag{7a}$$

$$\phi = \phi_g(\mathbf{x}) \quad \text{on } \Gamma_g \text{ (essential boundary condition)} \tag{7b}$$

$$\mathbf{K}\nabla\phi = \mathbf{q}(\mathbf{x}) \quad \text{on } \Gamma_h \text{ (natural boundary condition)}, \tag{7c}$$

where

$\mathbf{a}(\mathbf{x})$ = convection vector,
$\mathbf{K}(\mathbf{x})$ = diffusion tensor,
$f(\mathbf{x})$ = source term,
$\sigma(\mathbf{x})$ = linear term, and
$\Gamma = \Gamma_g \cup \Gamma_h$ is the boundary of the domain Ω.

Before proceeding, two categories of functions must be identified. The first set, known as the *trial functions*, will contain the solution function ϕ, and thus is required to satisfy the boundary condition of Eq. (7b). It will also be required that the trial functions are H^1 functions; that is, the function and its derivatives are integrable. The second set of functions, denoted by ϑ, comprises the *weighting functions*, which are also required to be members of H^1. Also, the weighting functions, w, are required to satisfy $w(\Gamma_g) = 0$. Practically, these requirements ensure that the integrals in the resulting weak form are all finite and that on the portions of the domain boundary on which the primary variable is fixed (Γ_g) the weighting function has the value zero.

In the basic weighted residual technique [6, 7], a suitable weak form may be derived by first multiplying the governing equation by an arbitrary weighting function and then integrating the result over the entire domain. The application of vector identities and the divergence theorem reduces the order of derivatives in some terms and also yields boundary integrals, into which known (linear or nonlinear) boundary conditions may be substituted. For the example convection-diffusion equation, the resulting weak form is:

Given $f(\mathbf{x})$, $\sigma(\mathbf{x})$, $\mathbf{a}(\mathbf{x})$, $\mathbf{K}(\mathbf{x})$, $\phi_g(\mathbf{x})$, and $\mathbf{q}(\mathbf{x})$, find $\phi \in \delta$ such that for all $w \in \vartheta$:

$$\int_\Omega w(\mathbf{a}\cdot\nabla\phi + \sigma\phi)\,d\Omega - \int_{\Gamma_h} w\mathbf{q}\cdot\mathbf{n}\,d\Gamma + \int_\Omega \nabla w\cdot\mathbf{K}\nabla\phi\,d\Omega = \int_\Omega wf\,d\Omega. \tag{8}$$

The domain, Ω, on which the problem is to be solved, is decomposed into a set of subdomains, or elements. On each element, approximate solution functions ϕ^h and weighting functions w^h will be chosen to be composed of a linear combination of *shape functions* and associated weighting factors,

$$\phi^h = \sum_{a=1}^{n} N_a(\mathbf{x})\phi_a \tag{9}$$

$$w^h = \sum_{a=1}^{n} N_a(\mathbf{x})w_a, \tag{10}$$

where the shape functions $N_a(\mathbf{x})$ are precribed to be simple polynomials and the ϕ_a are the solution values at discrete points. After evaluating and properly assembling all of the element weighted residual integrals, a global system of algebraic equations is obtained to be solved for the vector of unknowns $\boldsymbol{\phi}$ (a vector which contains the ϕ_a values for the assembly of all elements). The process described above is the standard (Galerkin) finite element method which produces the approximate solution ϕ^h.

The Galerkin method performs quite well for the convection-diffusion problem if the solution is regular (well-behaved), or if sharp internal or boundary layers exist in the solution and the finite element mesh is sufficiently refined to capture these layers. If changes in the exact solution occur over a scale-length that is small, compared with the element dimension,

then the Galerkin solution exhibits large-magnitude oscillations which propagate globally, destroying the accuracy of the method. This observation has prompted the development of finite element techniques specialized for convection-dominated problems, two of which are summarized below. With these methods, inaccuracies in representing sharp gradients are restricted to a small number of local elements, avoiding the large oscillations produced by the Galerkin method which destroy the accuracy of the solution on a global scale.

Modified Artificial Diffusion

To avoid the convection-dominated regime altogether in a multidimensional problem, it is reasonable to add anisotropic artificial diffusion based on the various velocity components and element dimensions,

$$k_x^* = k_x + \frac{|a_x| h_x}{2} \tag{11}$$

$$k_y^* = k_y + \frac{|a_y| h_y}{2}, \tag{12}$$

where h_x and h_y are the element dimensions in the x- and y-directions, respectively. This choice of artificial diffusion ensures that the element Peclet number is always less than or equal to unity, a situation for which the standard Galerkin method is adequate. Modified artificial diffusion will be used for the solution of the particle balance in the x-direction, as there is no physical D_x particle diffusion.

Streamline-Upwind/Petrov–Galerkin Method

The streamline upwind/Petrov–Galerkin (SU/PG) method [8] effectively adds artificial diffusion to the convection-dominated problem, but it does so only in the upwind direction by modifying the weighting functions such that more weighting is applied in the upwind direction. The SU/PG weighted residual formulation of the model convection-diffusion problem is:

Given $f(\mathbf{x})$, $\sigma(\mathbf{x})$, $\mathbf{a}(\mathbf{x})$, $\mathbf{K}(\mathbf{x})$, $\phi_g(\mathbf{x})$, and $\mathbf{q}(\mathbf{x})$, find $\phi^h \in \delta^h$ such that for all $w^h \in \vartheta^h$:

$$\begin{aligned} &\int_\Omega w^h(\mathbf{a}\cdot\nabla\phi^h + \sigma\phi^h)\,d\Omega - \int_\Gamma w^h \mathbf{q}\cdot\mathbf{n}\,d\Gamma \\ &\quad + \int_\Omega \nabla w^h \cdot \mathbf{K}\nabla\phi^h\,d\Omega + \sum_{e=1}^{n_{el}} \\ &\int_{\Omega_e} p(\mathbf{a}\cdot\nabla\phi^h - \nabla\cdot\mathbf{K}\nabla\phi^h + \sigma\phi^h - f)\,d\Omega \\ &\quad = \int_\Omega w^h f\,d\Omega. \end{aligned} \tag{13}$$

This form contains the standard Galerkin terms and adds a sum of integrals of the upwind weighting function, p, multiplied by the convection-diffusion residual. In this way the finite element solution is required to approximately satisfy the differential equation in a strong and weak sense, resulting in a method which is more stable and accurate than the Galerkin method. The form of p is given by [8]

$$p = \tau_1 \mathbf{a}\cdot\nabla w^h, \tag{14}$$

where τ_1 is a function of the element Peclet number, α (which is itself dependent on $|\mathbf{a}|$, h, and $\mathbf{K}$), and is chosen by the procedure in Ref. [9].

The anisotropy with regard to parallel and cross-field transport in the plasma edge region requires that modifications to the definition of the upwind weighting function be made. To illustrate the approach, consider the general convection-diffusion equation (7a) in two space dimensions with an anisotropic diffusion tensor:

$$a_x\frac{\partial\phi}{\partial x} + a_y\frac{\partial\phi}{\partial y} - \frac{\partial}{\partial x}\left(K_x\frac{\partial\phi}{\partial x}\right) - \frac{\partial}{\partial y}\left(K_y\frac{\partial\phi}{\partial y}\right) + \sigma\phi = f. \tag{15}$$

For typical problems of interest in edge modeling, K_x, K_y, a_x, and a_y may vary greatly over the domain, and K_x may be orders of magnitude greater than K_y. The problem is still two-dimensional since the cross-field (y) scale lengths are much smaller than the parallel (x) scale lengths.

For convection-dominated problems, optimal upwind finite element methods may be applied to Eq. (15). However, a choice must then be made as to the definition of the element Peclet number for use in obtaining the proper τ_1 values. One logical extension of the methods presented by Hughes *et al.* [9] is implemented with the condition that for isotropic K, the standard method is reproduced. In defining τ_1 for SU/PG, the equations for the direction-specific Peclet numbers (α_x and α_y), and the weighting parameters are

$$\alpha_x = \frac{|\mathbf{a}|h}{2K_x} \tag{16}$$

$$\alpha_y = \frac{|\mathbf{a}|h}{2K_y} \tag{17}$$

$$\tau_{1x} = \frac{1}{|\mathbf{b}|}\left[\coth\alpha_x - \frac{1}{\alpha_x}\right] \tag{18}$$

$$\tau_{1y} = \frac{1}{|\mathbf{b}|}\left[\coth\alpha_y - \frac{1}{\alpha_y}\right], \tag{19}$$

where $\mathbf{b} = (\mathbf{a}\cdot\nabla)\xi$ and $\xi(\mathbf{x})$ is the mapping of the actual element geometry in x–y space to a canonical bi-unit square element. The resulting anisotropic SU/PG weighting function becomes

$$p_{\mathrm{SUPG}} = \tau_{1x} a_x \frac{\partial w^h}{\partial x} + \tau_{1y} a_y \frac{\partial w^h}{\partial y}. \tag{20}$$

The procedure described above will be referred to in Section IV as "Anisotropic-1." Another choice is to fully isolate the x- and y-direction convection and diffusion terms. This involves defining the element Peclet numbers as

$$\alpha_x = \frac{|a_x| h_x}{2K_x} \tag{21}$$

$$\alpha_y = \frac{|a_y| h_y}{2K_y}. \tag{22}$$

The τ_{1x} and τ_{1y} parameters are then defined according to Eqs. (18) and (19), substituting b_x and b_y, respectively, for $\mathbf{b}$, for this variation on SU/PG, which will be called "Anisotropic-2." The ability of these methods to accurately model anisotropic transport will be addressed in Section IV.A for a general anisotropic convection-diffusion problem and for nonorthogonal meshes in Section IV.B. The important features of the anisotropic SU/PG methods are:

(a) diffusion is added only in the upwind direction,

(b) explicit control of the streamline derivative is provided, so that

(c) stability is added without sacrificing accuracy.

III.B. Weak Form of the Plasma Edge Equations

The finite element plasma edge code finds solutions to the following weak forms, in which Galerkin and modified artificial diffusion and/or SU/PG terms are included. In the parallel momentum, electron energy, and ion energy balances, the particle balance has been used to substitute S_n for $\nabla \cdot n\mathbf{V}$. This results in differential equations of the advective-diffusive form for which the SU/PG method was developed, but these weak forms are of course not unique.

Particle balance.

$$\begin{aligned}\int_\Omega &(w^h \nabla \cdot n^h \mathbf{w} + \nabla w^h \cdot \mathbf{D} \nabla n^h - w^h S_n)\, d\Omega \\ &+ \int_\Omega \frac{\partial w^h}{\partial x} D_x \frac{\partial n^h}{\partial x}\, d\Omega \\ &+ \int_{\Gamma_j} w^h \left(J_{\mathrm{CF}} + n^h D_p \frac{\partial T_i}{\partial y} - n^h v_{\mathrm{conv}} \right) \cdot \mathbf{n}_y\, d\Gamma \\ &+ \sum_{e=1}^{n_{el}} \int_{\Omega_e} p\, \mathrm{Res}(n^h)\, d\Omega = 0,\end{aligned} \tag{23a}$$

where

$$\mathrm{Res}(n^h) = \frac{\partial}{\partial x}(n^h u) + \frac{\partial}{\partial y}(n^h v) - S_n \tag{23b}$$

$$D_x = \frac{w_x h_x}{2} = \frac{u h_x}{2} = \text{modified artificial diffusion.} \tag{23c}$$

Applicable boundary conditions include:

Γ_g = portion of the boundary on which n^h is specified.

Γs = portion of the boundary on which $\nabla n^h \cdot \mathbf{n} = 0$ is specified (default),

Γj = portion of the boundary on which the cross-field particle flux is specified as J_{CF}.

Parallel momentum balance.

$$\begin{aligned}\int_\Omega &\left\{ w^h m_i n \mathbf{V} \cdot \nabla u_\parallel^h + \nabla w^h \cdot \boldsymbol{\eta} \nabla u_\parallel^h \right. \\ &\left. + w^h m_i S_n u_\parallel^h + w^h \frac{B_\theta}{B} \frac{\partial}{\partial x} [n(T_i + T_e)] \right\} d\Omega \\ &+ \sum_{e=1}^{n_{el}} \int_{\Omega_e} p\, \mathrm{Res}(u_\parallel^h)\, d\Omega = 0,\end{aligned} \tag{24a}$$

where

$$\begin{aligned}\mathrm{Res}(u_\parallel^h) = &\, m_i n \mathbf{V} \cdot \nabla u_\parallel^h - \nabla \cdot \boldsymbol{\eta} \nabla u_\parallel^h \\ &+ m_i S_n u_\parallel^h + \frac{B_\theta}{B} \frac{\partial}{\partial x} [n(T_i + T_e)].\end{aligned} \tag{24b}$$

Applicable boundary conditions include:

Γ_g = portion of the boundary on which $u_\parallel^h$ is specified.

Γ_s = portion of the boundary on which $\nabla u_\parallel^h \cdot \mathbf{n} = 0$ is specified (default),

Γ_{div} = portion of the boundary on which divertor-type boundary conditions are imposed, with $u_\parallel = C_s$ (the local soundspeed).

Electron energy balance.

$$\begin{aligned}\int_\Omega &w^h \left(\frac{3}{2} n \mathbf{V} \cdot \nabla T_e^h - T_e^h \mathbf{V} \cdot \nabla n + \frac{5}{2} S_n T_e^h \right. \\ &\left. + k_{eq}(T_e^h - T_i) - S_E^e \right) d\Omega + \int_\Omega \left(\nabla w^h \cdot \boldsymbol{\kappa}_e \nabla T_e^h \right) d\Omega \\ &+ \int_{\Gamma_q} w^h \left(q_{\mathrm{CF}} - \frac{5}{2} n v T_e^h \right) \mathbf{n}_y - \kappa_x^e \frac{\partial T_e^h}{\partial x} \mathbf{n}_x \Big) d\Gamma \Big) \\ &+ \int_{\Gamma_{\mathrm{div}}} \left(w^h \left(\delta_e - \frac{5}{2} \right) n \mathbf{V} T_e^h \cdot \mathbf{n} \right) d\Gamma \\ &+ \sum_{e=1}^{n_{el}} \int_{\Omega_e} p\, \mathrm{Res}(T_e^h)\, d\Omega = 0,\end{aligned} \tag{25a}$$

where

$$\mathrm{Res}(T_e^h) = \frac{3}{2} n\mathbf{V}\cdot\nabla T_e^h - \nabla\cdot\boldsymbol{\kappa}_e\nabla T_e^h - T_e^h\mathbf{V}\cdot\nabla n + \frac{5}{2}S_n T_e^h + k_{eq}(T_e^h - T_i) - S_E^e. \tag{25b}$$

Applicable boundary conditions include:

Γ_g = portion of the boundary on which T_e^h is specified.
Γ_s = portion of the boundary on which $\nabla T_e^h\cdot\mathbf{n} = 0$ is specified,
Γ_q = portion of the boundary on which the cross-field electron energy flux is specified as q_{CF}, and
Γ_{div} = portion of the boundary on which divertor-type boundary conditions are imposed, with the sheath electron energy transmission factor of δ_e.

Ion energy balance.

$$\begin{aligned}
&\int_\Omega w^h\left[\frac{5}{2}n\mathbf{V}\cdot\nabla T_i^h + \frac{5}{2}S_n T_i^h\right.\\
&\left.\quad + \frac{1}{2}m_i n\mathbf{V}\cdot\nabla u_\parallel^2 + \frac{1}{2}m_i u_\parallel^2 S_n\right]d\Omega\\
&\quad + \int_\Omega w^h[\mathbf{V}\cdot\nabla(nT_e^h)\\
&\quad - k_{eq}(T_e - T_i^h) - S_E^i]\,d\Omega\\
&\quad + \int_\Omega \nabla w^h\cdot\left[\boldsymbol{\kappa}_i\nabla T_i^h + \frac{1}{2}\eta\nabla u_\parallel^2\right]d\Omega\\
&\quad + \int_{\Gamma_s} w^h\left(-\frac{1}{2}\boldsymbol{\eta}\nabla u_\parallel^2\right)\cdot\mathbf{n}\,d\Gamma\\
&\quad + \int_{\Gamma_{div}} w^h\left(\delta_i - \frac{5}{2}\right)n\mathbf{V}T_i^h\cdot\mathbf{n}\,d\Gamma\Big)\\
&\quad + \int_{\Gamma_q} w^h\left[\left(q_{CF} - \frac{5}{2}nvT_i^h - \frac{1}{2}m_i n u_\parallel^2 v\right)\mathbf{n}_y\right.\\
&\quad \left.- \left(\kappa_x^i\frac{\partial T_i^h}{\partial x} + \frac{1}{2}\eta_x^i\frac{\partial u_\parallel^2}{\partial x}\right)\mathbf{n}_x\right]d\Gamma\Big)\\
&\quad + \sum_{e=1}^{n_{el}}\int_{\Omega_e} p\,\mathrm{Res}(T_i^h)\,d\Omega = 0,
\end{aligned} \tag{26a}$$

where

$$\begin{aligned}
\mathrm{Res}(T_i^h) &= \tfrac{5}{2}n\mathbf{V}\cdot\nabla T_i^h + \tfrac{5}{2}S_n T_i^h - \nabla\cdot\boldsymbol{\kappa}_i\nabla T_i^h\\
&\quad + \tfrac{1}{2}m_i n\mathbf{V}\cdot\nabla u_\parallel^2 + \tfrac{1}{2}m_i u_\parallel^2 S_n\\
&\quad - \tfrac{1}{2}\nabla\cdot\boldsymbol{\eta}\nabla u_\parallel^2 + \mathbf{V}\cdot\nabla(nT_e) - k_{eq}(T_e - T_i^h) - S_E^i.
\end{aligned} \tag{26b}$$

Applicable boundary conditions include:

Γ_g = portion of the boundary on which T_i^h is specified.
Γ_s = portion of the boundary on which $\nabla T_i^h\cdot\mathbf{n} = 0$ is specified,
Γ_q = portion of the boundary on which the cross-field ion energy flux is specified as q_{CF}, and
Γ_{div} = portion of the boundary on which divertor-type boundary conditions are imposed, with the sheath ion energy transmission factor of δ_i.

Neutral particle diffusion.

$$\begin{aligned}
&\int_\Omega[\nabla w^h\cdot\mathbf{D}_{no}\nabla n_o^h + w^h n n_o^h\langle\sigma v\rangle_{ei}]\,d\Omega\\
&\quad + \int_{\Gamma_\alpha} w^h\left[\frac{1}{2}\frac{1-\alpha}{1+\alpha}n_o^h\sqrt{\frac{T_i}{m_i}}\right]d\Gamma\\
&\quad - \int_{\Gamma_{div}} w^h R_p n\mathbf{V}\cdot\mathbf{n}\,d\Gamma = 0,
\end{aligned} \tag{27}$$

where only Galerkin terms are required due to the self-adjoint nature of the diffusion equation. Applicable boundary conditions include:

Γ_g = portion of the boundary on which n_o^h is specified.
Γ_α = portion of the boundary on which Marshak-type boundary conditions are applied with a neutral particle albedo α, and
Γ_{div} = portion of the boundary on which the neutral particle flux is set equal and opposite to the incident ion flux times the particle recycling coefficient, R_p.

In the current version of the finite element code for which results are presented in this paper, only quadrilateral elements and bilinear shape functions have been used. The SU/PG method was originally formulated for first-order shape functions only and has been successful enough in its application that quadratic, cubic, or higher order SU/PG elements have not been documented. As discussed in more detail in [9], the theoretical L_2 error in the convection-dominated case for the SU/PG method is $O(h^{k+1/2})$. (The parameter k is the degree of the complete polynomial used in the element interpolation functions, while h is the mesh parameter.) However, if the exact solution exhibits no internal or boundary layers, numerical results indicate optimal $O(h^{k+1})$ accuracy, the same order of accuracy produced by either the Galerkin or SU/PG method in the diffusion-dominated situation. For convection-dominated cases in which sharp layers are present, the theoretical error estimates are obtained by the SU/PG method if one considers the entire domain outside a small region surounding the layer. Again, the stability of SU/PG in such cases is in contrast to the Galerkin method for which numerical oscillations introduced by sharp layers propagate undamped throughout the entire solution.

III.C. Newton Nonlinear System Solver

The result of finite element discretization of the plasma edge equations is a system of highly nonlinear algebraic equations. In general, the system is of high dimension due to a typically large number of nodes, each with five variables to be determined: n, $u_\parallel$, T_i, T_e, and n_o. Referring to the solution vector for all the nodal degrees of freedom as $\boldsymbol{\phi}$, the finite element discretization of the system of differential equations leads to the nonlinear algebraic system:

$$\mathbf{F}(\boldsymbol{\phi}^*) = 0. \tag{28}$$

For an initial estimate, $\boldsymbol{\phi}^0$, Newton's method or a variation thereof is expected to perform well in iteratively solving Eq. (28) if $\boldsymbol{\phi}^0$ is sufficiently close to $\boldsymbol{\phi}^*$. Given an initial estimate, Newton's method forms a sequence of iterates by solving repeatedly the equation for $\mathbf{y}^k$, the correction vector

$$\frac{\partial \mathbf{F}(\boldsymbol{\phi}^k)}{\partial \boldsymbol{\phi}^k}(\boldsymbol{\phi}^{k+1} - \boldsymbol{\phi}^k) \equiv \mathbf{J}^k\mathbf{y}^k = -\mathbf{F}(\boldsymbol{\phi}^k), \tag{29}$$

where the Jacobian matrix $\mathbf{J}^k$ for iteration k has been defined as

$$\mathbf{J}^k = \{J_{ij}\} = \left\{\frac{\partial F_i^k}{\partial \phi_j^k}\right\}. \tag{30}$$

The sequence is terminated once the maximum relative correction is less than some tolerance ε, typically chosen to be 10^{-5}.

The residual vector $\mathbf{F}$ is a complicated function, representing the weighted residual integrals of the various weak forms and the appropriate boundary conditions. Therefore, the Jacobian matrix is numerically evaluated using a forward-difference approximation,

$$J_{ij} = \frac{\partial F_i}{\partial \phi_j} = \frac{F_i(..., \phi_j + \delta\phi_j, ...) - F_i(..., \phi_j, ...)}{\delta\phi_j}, \tag{31}$$

where $\delta\phi_j$ is a relatively small (10^{-6} to 10^{-5}) perturbation of the degree of freedom ϕ_j. Numerical $\mathbf{J}$ evaluation is less prone to programming errors than analytic forms for the complicated functions involved. Also, the program strucure is not affected by changes in the form of $\mathbf{F}$ (e.g., due to future modifications of the physics model). The Jacobian is evaluated on an element-by-element basis, so only potentially nonzero Jacobian entries are calculated. Therefore, the CPU time spent in Jacobian evaluation for a finite element mesh containing n_{el} elements is just proportional to n_{el}.

The matrix equation (29) is solved using the iterative algorithm GMRES (generalized minimum residual) developed by Saad and Schultz [11], which minimizes the residual norm $\|-\mathbf{F} - \mathbf{J}\mathbf{y}\|$. GMRES was developed for nonsymmetric indefinite systems and with proper preconditioning it outperforms other available techniques with respect to calculation of time and robustness. Preconditioning is applied by an incomplete LU factorization of $\mathbf{J}$. The CPU time required per linear system solution is proportional to n_{el}.

Several modifications of the standard Newton method have been employed to increase the radius of convergence or accelerate convergence:

(a) A search parameter modifies the updated solution vector to

$$\boldsymbol{\phi}^{k+1} = \boldsymbol{\phi}^k + s\mathbf{y}^k, \quad 0 < s \leq 1. \tag{32}$$

The method for determining the search parameter, s, is identical to the one used by Knoll [4], which is due to Winkler, Norman, and Mihalas [12] which limits the relative change in thermodynamic variables.

(b) The number of total Jacobian evaluations is reduced (e.g., calculating $\mathbf{J}$ in alternate iterations rather than in each iteration).

(c) Mesh sequencing [4] first solves the problem on a coarse mesh (which has a large radius of convergence), transfers the solution to be used as the initial guess for a finer mesh, and repeats the process until a solution is obtained on a mesh fine enough to provide acceptable accuracy.

The algorithms described above (the finite element discretization, Newton method, and GMRES linear system solver) have been implemented in a FORTRAN code written for use on Cray computers. Input consists of the standard finite element node coordinates, element connectivity, and boundary condition prescriptions. The solution output was postprocessed to obtain the 2D contour plots of plasma quantities and 1D profiles shown below.

IV. CODE VALIDATION AND APPLICATION TO ANGLED DIVERTOR PLATES

In order to establish the validity of the finite element method as programmed, each individual differential equation has been initially solved independently. For most of these tests, the choices of rectangular coordinates, constant transport coefficients, and boundary conditions allow the comparison of the finite element solution to an analytic exact solution. (Further details of these tests may be found in Ref. [10].) The purposes of these individual equation tests were to: (a) verify that the rate of convergence of the L_2 finite element error corresponds to the value predicted by theory; (b) test and compare the accuracy of Galerkin and SU/PG elements for a range of convection-diffusion situations. Below, the behavior of these finite element methods will be investigated for anisotropic transport situations on orthogonal and nonorthogonal meshes.

IV.A. Validation of the Anisotropic SU/PG Method

One peculiarity of plasma transport in magnetically confined configurations is the contrast in transport parallel and perpendicular to the magnetic field lines. The following test case involves a general two-dimensional convection-diffusion equation with constant coefficients described by the equation

$$u\frac{\partial \phi}{\partial x} + v\frac{\partial \phi}{\partial y} - D_x\frac{\partial^2 \phi}{dx^2} - D_y\frac{\partial^2 \phi}{dy^2} = 0 \quad \text{on } \Omega. \tag{33}$$

The domain Ω is taken to be the unit square. Essential boundary conditions on the entire boundary Γ are applied such that the exact solution

$$\phi(x, y) = \frac{e^{rx}e^{sy}}{(1 - e^r)(1 - e^s)} + \frac{e^{rx} - e^r(1 - e^{s(y-1)})}{(1 - e^r)(1 - e^{-s})} \tag{34}$$

is produced, where $r = u/D_x$ and $s = v/D_y$. The exact solution is characterized by $\phi(0, 0) = 1.0$, dropping to $\phi(x, y) = 0.0$ on the $x = 1$ and $y = 1$ boundaries in an either gradual or abrupt manner, depending on the convection-diffusion balance. The parameters r and s represent the degree of convection-dominance in the x- and y-directions, respectively. For this example, the following choices were made:

(a) $u = 5.0$

(b) $D_x = 1.0$

(c) $v = 1.0$

(d) $D_y = 0.01$.

so that $r = 5$ (moderately convection-dominated) and $s = 100$ (highly convection-dominated).

A uniform 10×10 finite element mesh was used to discretize the domain, on which bilinear shape functions and 2×2 Gauss quadrature were applied. This problem investigated the performance of three alternate finite element methods:

(a) modified artificial diffusion with $D_x^* = D_x + uh_x/2$ and $D_y^* = D_y + vh_y/2$,

(b) SU/PG using the Anisotropic-1 prescription of Section III.A, and

(c) SU/PG using the Anisotropic-2 formulas from Section III.A.

A summary of the results for this case is provided in Table I in terms of pointwise errors, showing the superior accuracy of the Anisotropic-2 SU/PG method relative to the other two methods, both in the (well-behaved) interior and near the sharp boundary layer. The modified artificial diffusion method is stable but over-diffuse, while the SU/PG Anisotropic-2 is more accurate than SU/PG Anisotropic-1. This occurs because for Anisotropic-1, the definition of τ_{1y} involves the magnitude of the vector velocity $|\mathbf{v}|$, rather than $|v|$ alone for Anisotropic-2. Consequently, since $|v| < |\mathbf{v}|$, the Anisotropic-1 definition gives a τ_{1y} value too low to fully eliminate the Galerkin oscillations near the sharp boundary layer at $y = 1$. Note that the Galerkin solution on such a coarse mesh exhibits large-scale oscillations throughout the domain, and so the results will not be presented.

TABLE I

Maximum Relative Pointwise Errors for Anisotropic SU/PG Test Case

Finite element method (10×10 grid)	Maximum relative pointwise error	
	Boundary layer	Interior
Modified artificial diffusion	19.8%	14.2%
Anisotropic-1 SU/PG	36.5%	14.4%
Anisotropic-2 SU/PG	16.1%	3.1%

IV.B. Nonorthogonal Mesh Tests

Because the physical boundaries of the plasma scrape-off region are typically not parallel or perpendicular to the poloidal magnetic field lines, the capability for nonorthogonal physical meshes is desirable, which is one reason for developing a finite element approach to the problem. The weighted residual derivation of the discrete equations involved only integrals over elements; no assumptions about the element shapes were made. Since the numerical integration scheme first maps an arbitrary quadrilateral element to a standard bi-unit square element, nonorthogonal elements are handled the same way as rectangular elements.

To verify the validity of non-rectangular elements, two test cases were devised in which the transport is strongly directional. Under these conditions, any artificial numerical transport introduced by a nonorthogonal mesh would be easily detected in the finite element solution, when compared with an orthogonal mesh solution. For the purposes of both tests, the ion energy equation solver was used.

Diffusion-Dominated Test Case

The first test, Case N1, involves conduction only, so that the equation being solved is

$$\kappa_x^i\frac{\partial^2 T_i}{\partial x^2} + \kappa_y^i\frac{\partial^2 T_i}{\partial y^2} = S_E^i. \tag{35}$$

The choice of boundary conditions was $T_i = 0$ on all boundaries. An energy source was chosen to be localized near the center of the mesh. If (x_c, y_c) are the coordinates of the geometric center of the domain, then

$$S_E^i(x, y) = 1.0 \times 10^{-18} \exp - \left[\frac{(x - x_c)^2 + (y - y_c)^2}{(0.02)^2}\right], \tag{36}$$

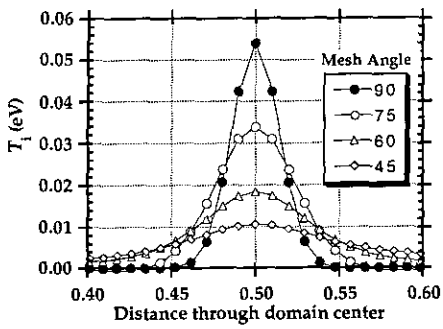

FIG. 1. Case N1. T_i vs y, element edges skew to the x-direction.

where S_E^i has the units of J $m^{-3}s^{-1}$. The conductance parameters used were $\kappa_x^i = 1.0$ $m^{-1}s^{-1}$ and $\kappa_y^i = 1.0 \times 10^{-8}$ $m^{-1}s^{-1}$, implying that the resulting T_i contours should be wide in the x-direction and very narrow in the y-direction.

A series of 40 × 40 Galerkin finite element meshes was applied to Case N1. In all cases the mesh was uniform in the x-direction, but elements were strongly concentrated near $y = 0.5$. The angle of the element edges to the x-axis was varied from 90° down to 45°. For this situation, in which all elements have two edges aligned with the dominant transport direction, the temperature profile is observed to remain essentially unchanged as the mesh angle proceeds from 90° to 45°. The maximum values of T_i remain within ~0.06% of the orthogonal mesh value, and the maximum pointwise difference in the finite element solutions is 2.1%.

A much different situation occurs when the dominant diffusive transport direction is skewed to the element edges. A series of 40 × 40 meshes was applied to Case N1 with $\kappa_x^i = 1.0 \times 10^{-8}$ $m^{-1}s^{-1}$ and $\kappa_y^i = 1.0$ $m^{-1}s^{-1}$, and the strongly anisotropic physical diffusion causes a profound spurious diffusion when nonorthogonal elements are used. Figure 1 displays the T_i profile for 90°, 75°, 60°, and 45° meshes, showing a progressive dampening of the peak and widening of the distribution. Therefore, for diffusion-dominated problems in which the diffusion tensor is highly anisotropic, the finite element methods investigated here require that element edges be approximately parallel to the dominant transport direction to yield an accurate solution.

Convection-Dominated Test Case

The situation is quite different when convection is the dominant mode of transport, because this is precisely the condition for which the SU/PG method was designed. For Case N2, a convection-dominated situation is created with $\mathbf{v} = 1.0\mathbf{e}_y$ m s^{-1}, $\kappa_x^i = \kappa_y^i = 1.0 \times 10^{-8}$ $m^{-1}s^{-1}$, and discontinuous inflow boundary conditions introduce an internal layer into the solution. Figure 2 displays the problem defined for a 20 × 20 orthogonal mesh, as well as the SU/PG solution, which is nodally exact. Another finite element mesh was applied to the equivalent problem in which the domain and element edges have been

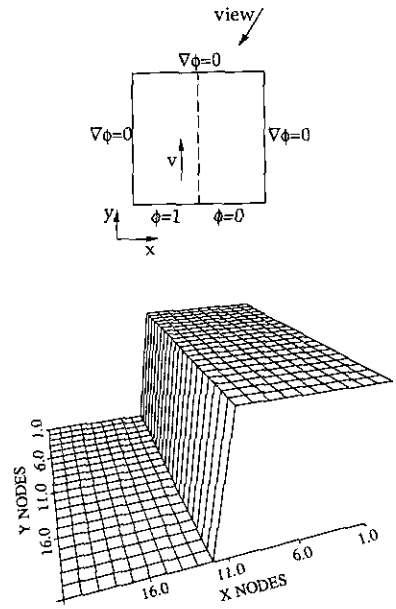

FIG. 2. Case N2. Problem diagram and exact solution on 90° mesh.

shifted from 90° to 60°. The exact solution is still a pure convection in the y-direction of the inflow boundary conditions, which in this case implies an internal layer skew to the mesh. Figure 3 displays the situation modeled as well as the SU/PG solution plotted on the 20 × 20 mesh. In this case, the application of a nonorthogonal mesh to this numerically difficult problem introduces no excessive spurious crosswind diffusion, with only localized oscillations.

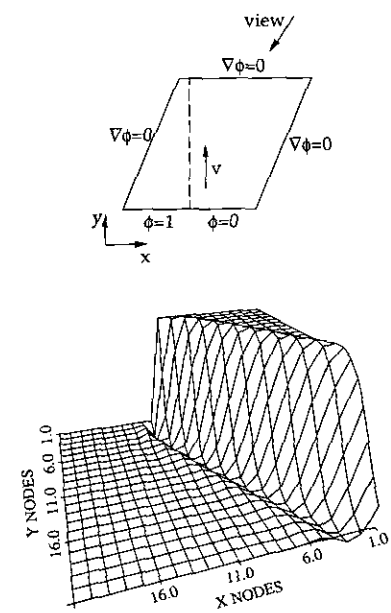

FIG. 3. Case N2. Problem diagram and SU/PG solution on 60° mesh.

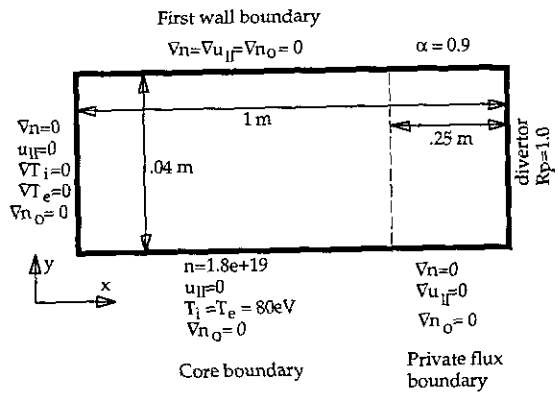

FIG. 4. Domain geometry for the plasma/neutral solution.

For typical edge plasmas, transport along the magnetic field is dominant, whether it be diffusive or convective. Orthogonal meshes created for use with existing plasma edge models always align themselves with the poloidal magnetic field to the extent possible. The divertor plate or limiter blade boundary is generally not normal to the magnetic field, causing problems for orthogonal mesh models. In the region near the divertor or limiter, the plasma is accelerating to the local soundspeed, so that parallel convection is the dominant process. The Petrov–Galerkin finite element methods (SU/PG) allow the use of nonorthogonal meshes in such regions to accurately model the physical boundary, as demonstrated by Case N2. Away from the divertor or limiter boundary, where (anisotropic) diffusion may dominate, an orthogonal finite element mesh is easily aligned with the preferred transport directions (along B_θ and $\perp B_\theta$).

IV.C. Self-Consistent Plasma/Neutral Solution

Once the single-equation tests described in Sections IV.A and IV.B were complete, the system of four plasma conservation equations was solved self-consistently on a rectangular ASDEX-like domain, and the results were compared to an identical B2 run. The Braginskii formulas were employed for parallel transport coefficients and cross-field coefficients were chosen as in [2]. The finite element results agree well with the B2 solution, differing at most by about 10% when compared pointwise. This test case also verified the Newton iteration method (including reduced J evaluation and mesh sequencing) and the GMRES linear system solver.

The next step is to couple the one-energy group neutral diffusion equation to the plasma equations. The computational domain is the rectangular region bounded by the poloidal midplane, divertor plate, first wall, and separatrix depicted in Fig. 4. All of the plasma ions incident on the divertor plate return as neutrals, and the flow of plasma particles across the separatrix is balanced by the flow of neutrals out the $\alpha = 0.9$ boundary. The additional parameters $D_n = 2.0$, $\eta_y^i = 0.2\, m_i n$, $\kappa_y^i = 0.2\, n$, $\kappa_y^e = 4\, n$, $\delta_i = 2.5$, and $B_\theta/B = 0.06$ were used. Consistent with the Braams analysis of this case, the following prescriptions were made for the neutral recycling model:

(a) $\varepsilon_i = 5$ eV/ionization (ion energy gain)

(b) $\varepsilon_e = -25$ eV/ionization (electron energy loss)

(c) $\langle \sigma v \rangle_{ie} = 3 \times 10^{-14} a^2/(3 + a^2)$, where $a = T_e(\text{eV})/10$

(d) $\langle \sigma v \rangle_{cx} = 1 \times 10^{-14} T_e^{1/3}$

(e) $m_i = 1.5\ m_p$ (where m_p is the proton mass, representing an equal mixture of hydrogen and deuterium)

Boundary conditions on the plasma quantities remain essentially as shown in Fig. 4, although the following modifications are made for the private flux, first wall, and divertor plate boundaries for comparison with published B2 and NEWEDGE results:

(a) B2 boundary conditions:
Private flux: $\nabla T_i = \nabla T_e = 0$
First wall: $T_i = T_e = 2$ eV (for $0 \leq x \leq 0.75$ m)
Divertor plate: $q_i = \delta_i n u T_i + \frac{1}{2} m_i n u C_s^2$, $\delta_e = 4.0$.

(b) NEWEDGE boundary conditions:
Private flux: $\nabla T_i = T_i/\lambda$, $\nabla T_e = T_e/\lambda$, where λ is the density gradient scale length [3]
First wall: $\nabla T_i = \nabla T_e = 0$
Divertor plate: $q_i = \delta_i n u T_i$, $\delta_e = 4.5$. (To be consistent with NEWEDGE, ion kinetic, and viscous effects are omitted from the ion energy balance completely.)

A series of graded finite element meshes was applied to the problem using the SU/PG (Anisotropic-2) method. The first mesh, for which uniform initial estimates of n, $u_\parallel$, T_i, T_e, and n_o were used, is the 14 × 5 mesh displayed in Fig. 5. Succeeding

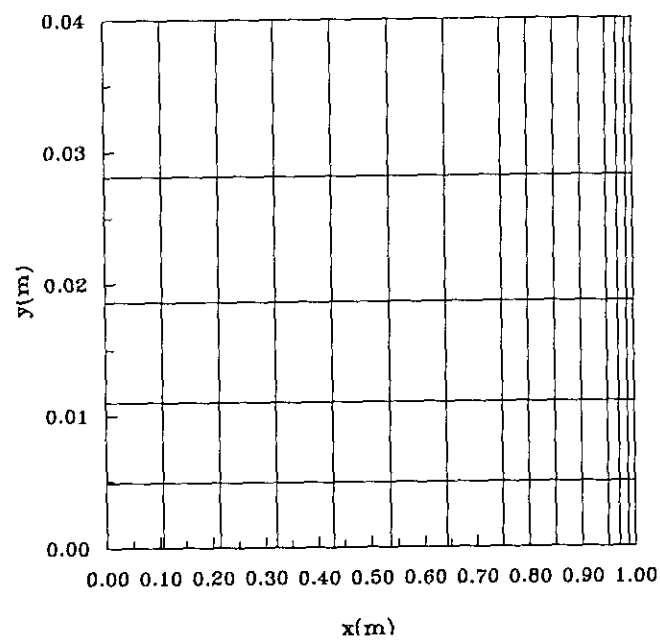

FIG. 5. Initial 14 × 5 finite element mesh for the plasma/neutral solution.

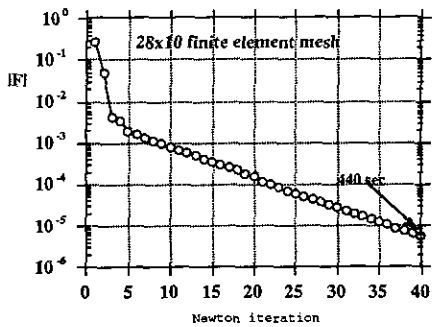

FIG. 6. Residual vs Newton iteration for the plasma/neutral solution on 28×10 mesh.

meshes (e.g., 28×10 and 56×20) were constructed with the interpolated solution from the previous mesh used as the initial solution estimate. In all cases bilinear shape functions and 2×2 Gauss quadrature numerical integration were employed.

Figure 6 displays the typical Newton convergence behavior for the consistent solution of the full plasma/neutral system of equations, in this case for the 28×10 mesh. This case required 440 s on the Cray-2 C-machine at the National Energy Research Supercomputer Center, with the vast majority of the computing time spent on numerical evaluation of the Jacobian matrix. The GMRES linear solver is quite efficient and accounts for a small portion (<10%) of the total computing time. Future optimization efforts should therefore aim at streamlining the Jacobian evaluation or limiting the number of evaluations.

Figures 7 and 8 display the SU/PG solution contours for ion density and electron temperature calculated on a 56×20 mesh for the case with NEWEDGE plasma boundary conditions. The ion density exhibits a sharp increase directly in front of the divertor plate due to the highly localized neutral particle recycling zone, while electron temperatures show the rapid decrease from the x-point to the divertor plate indicative of localized neutral recycling. The changes in physics and boundary conditions from the NEWEDGE-like case to the B2-like case manifest themselves in the self-consistent plasma solution, seen in the density and electron temperature contours of Figures 9 and 10. The imposition of low temperature essential boundary conditions at the first wall leads to the production of a relatively large region of recirculating flow and thus lowers the peak ion density near the plate.

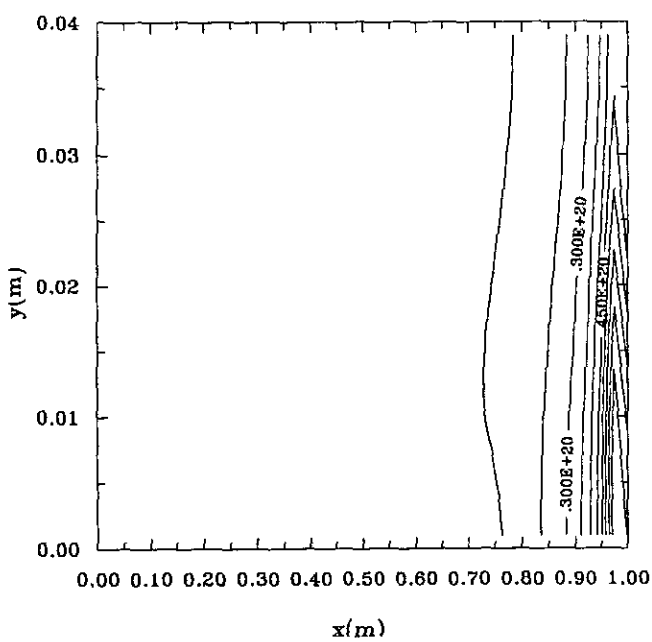

FIG. 7. Ion density contours for the plasma/neutral solution with NEWEDGE-like boundary conditions (contour increment = 5.0×10^{18} m^{-3}).

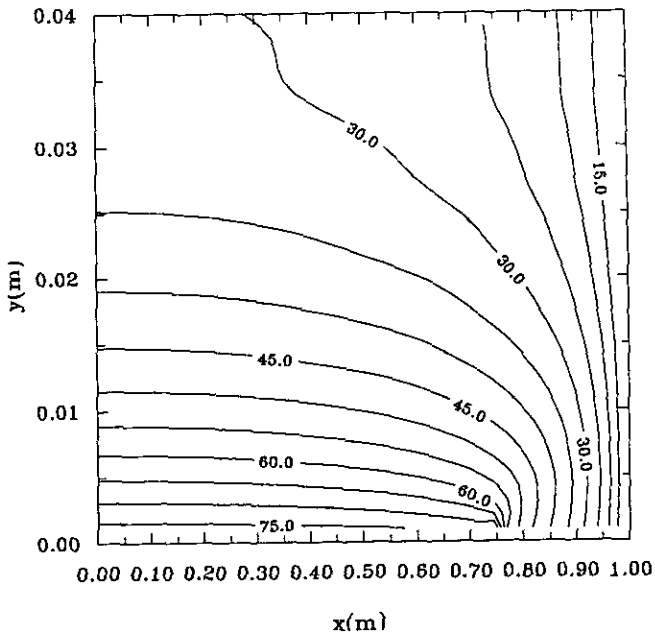

FIG. 8. Electron temperature contours for the plasma/neutral solution with NEWEDGE-like boundary conditions (contour increment = 5 eV).

Table II displays the near-plate quantities computed by the finite element code, B2, and NEWEDGE for this case. The finite element and NEWEDGE results reveal that the peak density occurs about 2-cm upwind of the divertor plate, for which the NEWEDGE central differencing solution gives 9.0 $\times 10^{19}$ m^{-3} compared to 8.8×10^{19} m^{-3} from the finite element code. Turning to the B2 comparison, the 30% discrepancies between the codes are acceptable considering that the B2 code uses a much simpler analytic neutral particle model. It should also be noted that the published B2 values were the result of a two-species (deuterium and hydrogen) calculation, while the finite element code modeled one ion species with the average mass of D and H.

The purpose of this test case for the finite element code was to demonstrate its performance for both sets of boundary

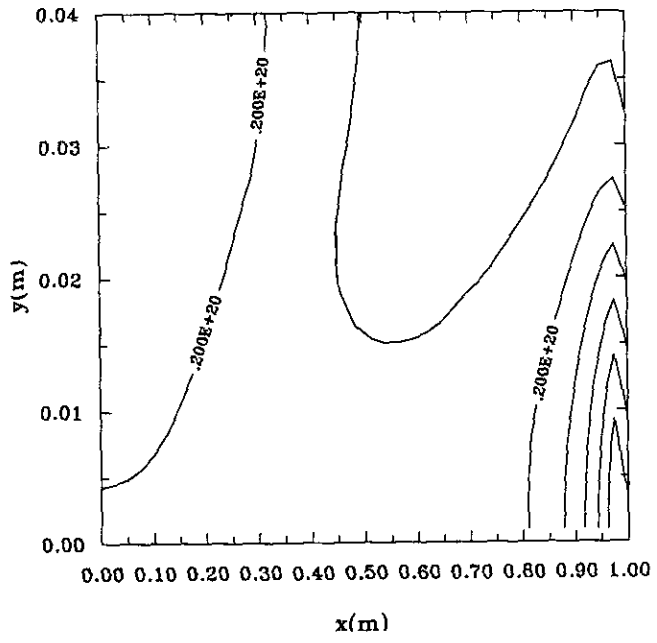

FIG. 9. Ion density contours for the plasma/neutral solution with B2-like boundary conditions (contour increment = 5.0×10^{18} m^{-3}).

conditions appearing in the published results of B2 and NEWEDGE. Given the proper boundary conditions, the finite element code agrees qualitatively and quantitatively with both the NEWEDGE and B2 codes. Finally, this also points out the real differences between the cases modeled by Braams and Knoll,

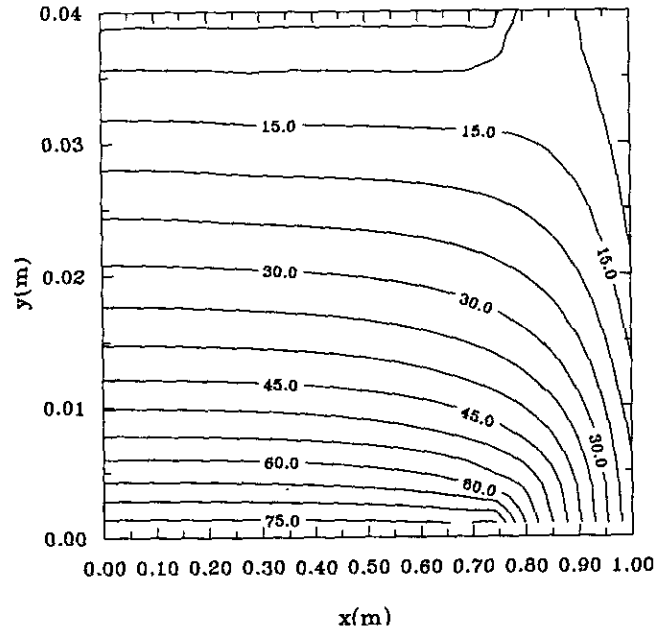

FIG. 10. Electron temperature contours for the plasma/neutral solution with B2-like boundary conditions (contour increment = 5 eV).

TABLE II

Comparison of Near-Plate Results for B2, NEWEDGE, and Finite Element Codes

Code	Peak n (m^{-3})	T_i (eV)	T_e (eV)	Peak q''(MW/m^2)
NEWEDGE	9.0×10^{19}	—	—	1.75
Finite element	8.8×10^{19}	14.7	5.0	1.42
B2	5.5×10^{19}	13	19	2.9
Finite element	4.6×10^{19}	9.1	22.0	2.13

and so in comparing edge plasma codes, the physical situations modeled must be as similar as possible to yield meaningful information.

IV.D. Effect of Angled Divertor Plates

The situation in which the boundary is orthogonal to the poloidal magnetic field lines never occurs in realistic divertor or limiter configurations, and this fact was a primary motivation for developing a finite element edge plasma model. An ad hoc solution to this problem is to scale the calculated plasma heat flux to the divertor plate by the sine of the angle between the poloidal magnetic field lines and the divertor plate surface. The finite element method is capable of representing the nonorthogonal divertor boundary accurately and therefore treat the problem more consistently.

To investigate the consequences of inclined divertor plates, the physical problem of Section IV.C is recalled, so that the geometry, transport coefficients, and boundary conditions remain as described for the NEWEDGE-like case. The results from the case in which the divertor plate is normal to B_θ will be compared with the results from simulations in which the divertor plate/separatrix angles are $+60°$ and $-60°$. Figure 11 illustrates the domain geometry for the three divertor plate inclinations.

The primary influence of the divertor plate inclination appears in the neutral particle balance, through the plate recycling boundary condition. Neutrals formed at the plate are effectively emitted normal to the divertor plate, so that the $+60°$ divertor

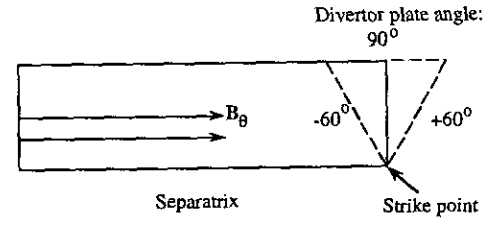

FIG. 11. Domain geometry for the angled divertor case.

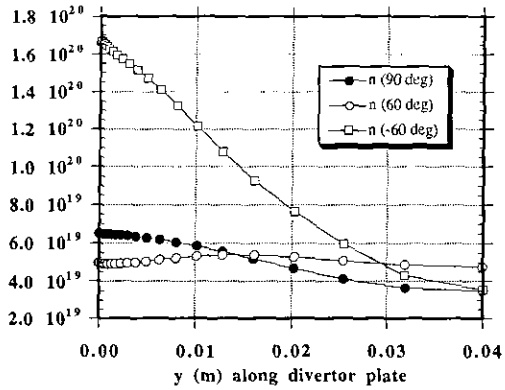

FIG. 12. Ion density profile at divertor plate for the angled divertor case.

shifts the ionization peak outward from the separatrix, while the $-60°$ divertor tends to focus the neutrals toward the separatrix.

Figure 12 displays the ion density profile at the divertor plate for the three divertor plate orientations. While the strike point density is reduced by 23% from the 90° to 60° divertor plate solutions, the $-60°$ divertor results show a factor of 2.5 increase in density. The changes in plasma density distributions near the plate also affect the ion and electron temperatures and thus the heat flux to the divertor surface. Figure 13 displays the heat flux normal to the divertor plate surface for the three plate angles. Also shown as a dotted line is the 90° divertor heat flux scaled by the sin 60° geometric factor which would be applied to calculations from an orthogonal boundary model. The $-60°$ divertor plate drastically reduces the total divertor heat flux in this simulation. This is due to a combination of the private flux temperature scale-length NEWEDGE-like boundary condition and the density dependence of the anomalous cross-field conductances, $\kappa_\parallel^e$ and $\kappa_\perp^i$. As the density along the private flux boundary increases, the cross-field thermal conductivity of the plasma increases and more energy is allowed to escape across the separatrix, thus reducing the energy transported along the field lines to the divertor plate. The focusing of the ion density toward the separatrix seen with the $-60°$ divertor serves to

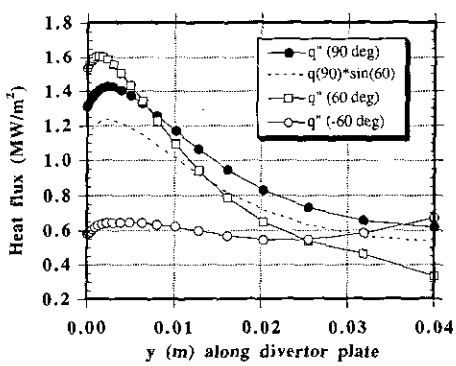

FIG. 13. Heat flux profile at divertor plate for the angled divertor case.

increase the importance of the private flux boundary condition, and a more realistic simulation would extend the mesh beyond the separatrix to a physical wall to eliminate the temperature scale-length assumption. Nonetheless, the divertor plate angle directly affects the neutral ionization source and thus impacts the ion density buildup near the plate which is critical in distributing the plasma energy content. The effects of irregular boundary geometry (e.g., angled divertor plates) on the entire edge plasma/neutral system must be incorporated in a self-consistent way, as has been accomplished with the finite element model.

V. SUMMARY AND FUTURE WORK

To yield an accurate approximate solution to the plasma conservation equations which contain significant first derivatives, the modified artificial diffusion and streamline-upwind/Petrov–Galerkin (SU/PG) finite element methods have been implemented. Anisotropic upwind weighting provides a means to numerically stabilize the anisotropic convection-diffusion behavior of the edge plasma. The standard Galerkin method is adequate to model the one-energy-group neutral particle diffusion equation. The finite element method transforms the system of plasma/neutral equations into a nonlinear system of algebraic equations, which is solved by a damped modified Newton iteration scheme.

As with any new computational model, the finite element plasma edge code has undergone several phases of testing designed not only to debug it but to identify its capabilities and limitations. Tests in which highly anisotropic convection-dominated transport is modeled on a nonorthogonal mesh confirmed the ability of finite elements to represent the irregular boundary geometry of the edge region. A test case attempting to reproduce published B2 and NEWEDGE results succeeded in benchmarking the finite element code to both sets of results independently, as well as highlighting the importance of boundary conditions in determining the computed solution. Finally, the self-consistent modeling of inclined divertor plates pointed out the importance of boundary geometry and showed that the angling of divertor plates introduces effects more pronounced than just a linear reduction in the particle and energy fluxes to the plate.

Specific near-term modifications to the finite element code include:

(a) an improved neutrals model such as a two-group treatment including charge-exchange (fast) neutrals and wall-released Franck–Condon (slow) neutrals,

(b) implementation of a nonorthogonal grid generator which utilizes magnetic geometry and smoothly incorporates the actual plasma-facing surface boundary, and

(c) formulation of the weighted residual statements to directly incorporate the (R, Z) geometry provided by the nonorthogonal grid generator of item (b) and avoid the translation to x–y geometry.

The solution to the problem of dealing with irregular boundary

geometry is offered by finite element methods. However, many other improvements and additions (such as consistent boundary conditions, impurities, noncoronal radiation, and cross-field transport models) are needed before a truly satisfactory edge model is available.

ACKNOWLEDGMENTS

The GMRES linear system solver routine was made available by Youcef Saad and suggested by Professor Mark Shephard of RPI. This work was performed under appointment to the Magnetic Fusion Energy Technology Fellowship program which is administered for the U.S. Department of Energy by the Oak Ridge Institute for Science and Education.

REFERENCES

1. T. Kuroda *et al.*, *ITER Plasma Facing Components*, ITER Documentation Series, No. 30 (International Atomic Energy Agency, Vienna, 1991).
2. B. J. Braams, "A Multi-fluid Code for Simulation of the Edge Plasma in Tokamaks," NET Report EUR-FU/XII-80/87/68, January 1987 (unpublished).
3. E. Vold, "Transport in the Tokamak Plasma Edge," Ph.D. thesis, University of California, Los Angeles, 1989 (unpublished).
4. D. Knoll, A. K. Prinja, and R. B. Campbell, *J. Comput. Phys.* **116** (1995).
5. S. I. Braginskii, Transport processes in a plasma, in *Reviews of Plasma Physics, Vol. 1* edited by M. A. Leontovich (Consultants Bureau, New York, 1965), p. 205.
6. T. J. R. Hughes, *The Finite Element Method, Linear Static and Dynamic Finite Element Analysis* (Prentice-Hall, Englewood Cliffs, NJ, 1987).
7. B. A. Finlayson, *The Method of Weighted Residuals and Variational Principles* (Academic Press, New York, 1972).
8. A. N. Brooks and T. J. R. Hughes, *Comput. Methods Appl. Mech. Engrg.* **32,** 199 (1982).
9. T. J. R. Hughes, M. Mallet, and A. Mizukami, *Comput. Methods Appl. Mech. Engrg.* **54,** 341 (1986).
10. R. A. Vesey, "A Finite Element Approach to Edge Plasma Modeling," Ph.D. thesis, Rensselaer Polytechnic Institute, Troy, NY, 1992 (unpublished).
11. Y. Saad and M. H. Schultz, *SIAM J. Sci. Statist. Comput.* **3,** 856 (1986).
12. K-H. A. Winkler, M. L. Norman, and D.Mihalas, Implicit adaptive-grid radiation hydrodynamics, in *Multiple Time Scales*, edited by J. U. Brackbill and B. I. Cohen (Academic Press, Inc., New York, 1985).